Inorganic Chemistry

Article

pubs.acs.org/IC

Surfactant Media To Grow New Crystalline Cobalt 1,3,5-Benzenetricarboxylate Metal–Organic Frameworks

Hai-Sheng Lu,[†,‡,§] Linlu Bai,[⊥,§] Wei-Wei Xiong,[‡] Peizhou Li,[∥] Junfeng Ding,[¶] Guodong Zhang,[‡] Tom Wu,[¶] Yanli Zhao,[∥] Jong-Min Lee,[⊥] Yanhui Yang,*[,⊥] Baoyou Geng,*[,†] and Qichun Zhang*[,‡]

[†]College of Chemistry and Materials Science, The Key Laboratory of Functional Molecular Solids, Ministry of Education, Anhui Laboratory of Molecular-Based Materials, Centre for Nano Science and Technology, Anhui Normal University, Wuhu 241000, P. R. China

[‡]School of Materials Science and Engineering and [⊥]School of Chemical and Biomedical Engineering, Nanyang Technological University, Singapore 639798, Singapore

[∥]School of Physical and Mathematical Sciences, Nanyang Technological University, Singapore 637371, Singapore

[¶]Physical Sciences and Engineering Division, King Abdullah University of Science and Technology, Thuwal 23955-6900, Saudi Arabia

Supporting Information

ABSTRACT: In this report, three new metal–organic frameworks (MOFs), $[Co_3(\mu_3\text{-}OH)(HBTC)(BTC)_2Co(HBTC)]\cdot(HTEA)_3\cdot H_2O$ (**NTU-Z30**), $[Co(BTC)]\cdot HTEA\cdot H_2O$ (**NTU-Z31**), $[Co_3(BTC)_4]\cdot(HTEA)_4$ (**NTU-Z32**), where H_3BTC = 1,3,5-benzenetricarboxylic acid, TEA = triethylamine, and NTU = Nanyang Technological University, have been successfully synthesized under surfactant media and have been carefully characterized by single-crystal X-ray diffraction, powder X-ray diffraction, thermogravimetric analysis, and IR spectromtry. **NTU-Z30** has an unusual trimeric $[Co_3(\mu_3\text{-}OH)(COO)_7]$ secondary building unit (SBU), which is different from the well-known trimeric $[Co_3O(COO)_6]$ SBU. The topology studies indicate that **NTU-Z30** and **NTU-Z32** possess two new topologies, 3,3,6,7-c net and 2,8-c net, respectively, while **NTU-Z31** has a known topology **rtl** type (3,6-c net). Magnetic analyses show that all three materials have weak antiferromagnetic behavior. Furthermore, **NTU-Z30** has been selected as the heterogeneous catalyst for the aerobic epoxidation of alkene, and our results show that this material exhibits excellent catalytic activity as well as good stability. Our success in growing new crystalline cobalt 1,3,5-benzenetricarboxylate MOFs under surfactant media could pave a new road to preparing new diverse crystalline inorganic materials through a surfactant-thermal method.

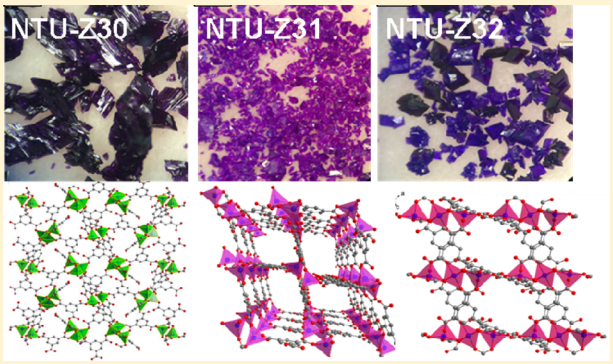

INTRODUCTION

In the past 2 decades, big achievement has been witnessed in metal–organic frameworks (MOFs)[1] because MOFs not only have diverse structures with tunable porous characteristics[1] and intriguing topologies but also have possible applications in gas separation and storage,[2] nonlinear optics,[3] catalysis,[4] chemical sensors,[5] magnetism,[6] ion exchange, and biology.[4a,e,7] Generally, MOFs with interesting structures and diverse properties can be prepared via several different methods including solvothermal,[8] ionothermal,[7b,9] and urea-thermal methods.[10] However, all of these methods have to involve the utilization of organic small molecules (or salts) as solvents, which will bring several disadvantages during synthesis: (1) low boiling points of organic solvents (except ionic liquids, ILs) might set up a limitation on the reaction temperature; (2) organic solvents could cause serious health and environmental problems; (3) organic solvents have less efficiency in directing crystal growth because of their weak interactions with as-growing crystal facets; (4) some greener solvents such as ILs have limited commercially available sources. Thus, developing a new synthetic strategy to avoid these disadvantages is highly desirable.

Logically, surfactants should be able to direct the growth of bulky crystals because they have been widely proven as efficient templates to determine the morphologies of nanostructures.[11] In fact, surfactant-thermal strategy has already been demonstrated as a novel synthetic method to produce new crystalline materials[1e,f,11a,12−14] because of their charming advantages.[11f,g] In addition, the low price and more choices from commercially available sources have made surfactants as reaction media more attractive compared with ILs and ureas.[15] Previously, Wang and co-workers have already demonstrated that nanoporous zeolites can be prepared by employing surfactants as directing agents.[13a] In our previous research, we also show that reactions under surfactant media can be a powerful platform to direct single-

Received: May 15, 2014
Published: August 7, 2014

   dx.doi.org/10.1021/ic5011133 | *Inorg. Chem.* 2014, 53, 8529−8537

crystal growth of MOFs and chalcogenides.[1e,f,11a,12,14] For example, we have prepared several new crystalline MOFs with diverse structures under surfactant-thermal condition.[11a,14] In addition, the effect of surfactants on crystal growth is also investigated.[16]

In our continuous research, we are interested in investigating the connecting modes between 1,3,5-benzenetricarboxylate acid (BTC) linkers and cobalt ions under surfactant media. We hope that surfactants could not only control the formation of different second building units (SBUs) but also further affect the connection of in situ generated SBUs to construct frameworks. Moreover, the as-prepared new cobalt-based MOFs might act as efficient catalysts for the epoxidation of alkenes.[2e] Herein, we report the synthesis, characterization, and physical properties of three novel cobalt-based MOFs: $[Co_3(\mu_3\text{-}OH)(HBTC)(BTC)_2Co(HBTC)]\cdot(HTEA)_3\cdot H_2O$ (**NTU-Z30**), $[Co(BTC)]\cdot HTEA\cdot H_2O$ (**NTU-Z31**), and $[Co_3(BTC)_4]\cdot(HTEA)_4$ (**NTU-Z32**).

EXPERIMENTAL SECTION

Materials. All reagents were obtained from Aldrich, TCI Chemical, and Alfa Aesar and were used without further treatment.

Characterization. Powder X-ray diffraction (PXRD) data were recorded on a Bruker D8 Advance diffractometer with graphite-monochromatized Cu Kα radiation (λ = 1.54178 Å) and a step size of 0.05°. Elemental analysis (EA) was performed on a EuroVector Euro EA elemental analyzer. Fourier transform infrared (FTIR) spectra were recorded from KBr pellets using a PerkinElmer FTIR Spectrum GX spectrometer. Inductively coupled plasma mass spectrometry (ICP-MS) tests were done on an ICP-MS Agilent 7700 spectrometer before the samples were digested by the CEM MDS-5 microwave oven. Thermogravimetric analysis (TGA) was carried out on a TA Instrument Q500-TGA analyzer at a heating rate of 10 °C min^{-1} up to 850 °C under a N_2 atmosphere. X-ray diffraction pattern simulation was obtained through the single-crystal data and diffraction-crystal module of the *Diamond* program (version 3.0) available free of charge via the Internet http://www.crystalimpact.com/diamond/Default.htm. Crystal pictures, PXRD, TGA, net topologies, FTIR, and thermal ellipsoid plots of all MOFs are provided in the Supporting Information (SI) as Figures S1−S8.

Synthesis of MOFs. ***NTU-Z30***. A mixture of $Co(NO_3)_2\cdot H_2O$ (1 mmol, 0.291g), 1,3,5-benzenetricarboxylic acid (H_3BTC; 0.5 mmol, 0.105 g), triethylamine (TEA; 1 mL), and 4 mL of nonanoic acid was put into a 23 mL autoclave and heated at 160 °C for 6 days. Then, the reaction was naturally cooled and washed with acetone to give purple-black bar crystals of **NTU-Z30** (see the photograph of Figure S1a, SI). Yield: 80% (based on H_3BTC). EA and ICP analysis for $Co_4C_{54}H_{62}N_3O_{26}$ (1404.79): Co, 16.92; C, 46.08; H, 4.55; N, 3.05 (calcd: Co, 16.80; C, 46.13; H, 4.41; N, 2.99). IR (KBr pellet): 676(vs), 719(s), 758(s), 823(s), 879(s), 939(s), 1051(s), 1099(s), 1186(m), 1249(m), 1367(m), 1441(m), 1492(s), 1561(m), 1613(m), 1635(m), 1721(m), 2857(s), 2926(s), 3017(s), 3415(vs).

NTU-Z31 and NTU-Z32. A synthesis procedure similar to that for preparing **NTU-Z30** has been adopted but with a difference ratio of raw materials. For **NTU-Z31**, a mixture of $Co(NO_3)_2\cdot H_2O$ (0. 5 mmol, 0.145 g), H_3BTC (1 mmol, 0.210 g), TEA (2.5 mL), and 2.5 mL of nonanoic acid was employed, and red bar crystals of **NTU-Z31** (see the photograph of Figure S1b, SI) were obtained in 70% yield (based on H_3BTC). EA and ICP analysis for $CoC_{15}H_{21}NO_7$ (386.26): Co, 15.21; C, 46.53; H, 1.55; N, 4.17 (calcd: Co, 15.27; C, 46.60; H, 1.41; N, 4.26). IR (KBr pellet): 685(vs), 715(s), 762(s), 827(s), 874(s), 1048(vs), 1181(vs), 1259(s), 1367(m), 1436(m), 1492(s), 1561(m), 1618(m), 1696(s), 2491(vs), 2680(s), 2857(s), 2926(s), 3112(vs), 3411(vs). For **NTU- Z32**, a mixture of $Co(NO_3)_2\cdot H_2O$ (0.5 mmol, 0.145 g), H_3BTC (0.5 mmol, 0.105 g), TEA (1 mL), and 4 mL of nonanoic acid was used, and purple prism crystals of **NTU-Z32** were obtained (see the photograph of Figure S1c, SI). Yield: 80% (based on H_3BTC). EA and ICP analysis for $Co_3C_{60}H_{76}N_4O_{24}$ (1414.04): Co, 12.56; C, 50.97; H, 5.17; N, 4.07 (calcd: Co, 12.52; C, 50.92; H, 5.37; N, 3.96). IR (KBr pellet): 685(vs), 715(s), 762(s), 1181(s), 1259(s), 1367(m), 1432(m), 1488(s), 1561(m), 1622(m), 1691(s), 2491(vs), 2676(s), 2737(vs), 2857(vs), 2931(s), 2983(s), 3112(s), 3411(vs).

Single-Crystal X-ray Crystallography. The single-crystal X-ray diffraction data were collected on a Bruker APEX II CCD diffractometer with graphite-monochromated Cu Kα radiation (λ = 1.54178 Å). All structures were solved by direct methods and refined by full-matrix least-squares cycles in *SHELX-97*. All H atoms were calculated and refined using a riding model.

Catalytic Epoxidation. The epoxidation of different alkenes involving O_2 gas was performed in a three-neck glass flask equipped with a stirring bar and a reflux condenser. Typically, 2.5 mg of **NTU-Z30**, 1 mmol of substrate, and 15 mL of *N*,*N*′-dimethylformamide (DMF) were charged into the above flask. Under vigorous stirring, the mixture was heated to the desired reaction temperature and a stream of O_2 gas (30 mL min^{-1}) was bubbled into the glass flask to initiate epoxidation.

After catalysis by **NTU-Z30**, the liquid solution was separated and analyzed by a gas chromatograph (Agilent 6890) using dodecane as the internal standard.[2e] All as-obtained compounds were analyzed and identified on a gas chromatograph−mass spectrometer (Agilent, GC 6890N, MS 5973 inert). Solid-state UV−vis diffuse-reflectance spectra were recorded on a model UV-2501 PC at room temperature using a $BaSO_4$ pallet as the standard (100% reflectance).

For reaction time effect examination, the reaction was performed with 1 h intervals. The procedure of hot filtration was same as what we reported previously.[2e]

RESULTS AND DISCUSSION

Synthesis. Because surfactants are very powerful to direct the growth of inorganic or organic materials at the nano/microscale, it is reasonable to employ surfactants to control the crystal growth at the macroscale. Surfactants have both hydrophilic and hydrophobic groups, which not only enhance the solubility of inorganic salts and organic linkers but also efficiently direct crystal growth through strong interaction between the crystal faces and surfactants. It is worth noting that the final products under surfactant-thermal synthesis are normally unpredictable because this type of synthesis is a relatively complex process. In addition, the ratio of starting compounds also plays an important role in control of the formation of new materials and their crystal growth. For example, the reaction mixtures with Co^{2+}: H_3BTC = 2:1 can produce **NTU-Z30**, while Co^{2+}:H_3BTC = 1:1 gives **NTU-Z32**. In fact, our experimental conditions reported here are optimized, and the other conditions that we have tried have been summarized and provided in Table S1 (SI). It clearly indicates that, without surfactants, no MOF crystals or a small amount of poor MOF crystals are available. In addition, PXRD has been employed to confirm the phase purities of all as-prepared crystals (Figure S2, SI). Note that because the channels of MOFs reported here have been occupied by organic cations and removing these cations will cause the collapse of MOFs, it might not be necessary to measure the pores' sizes. In fact, **NTU-Z30** has been tried, and no pores were observed without removing cations.

Structure Description of NTU-Z30. The structure determined by a single-crystal X-ray diffractometer shows that **NTU-Z30** has the monoclinic space group $P2_1/c$ with two different SBUs (Figure 1a,b): one is a new trimeric $[Co_3(\mu_3\text{-}OH)(COO)_7]$ SBU (Figure 1a), different from the reported trimeric $[M_3O(COO)_6]$ SBU (M = Co, Cr, Mn, Ni, Cd),[17] which consists of three Co^{2+} atoms coordinating with seven

dx.doi.org/10.1021/ic5011133 | *Inorg. Chem.* 2014, 53, 8529−8537

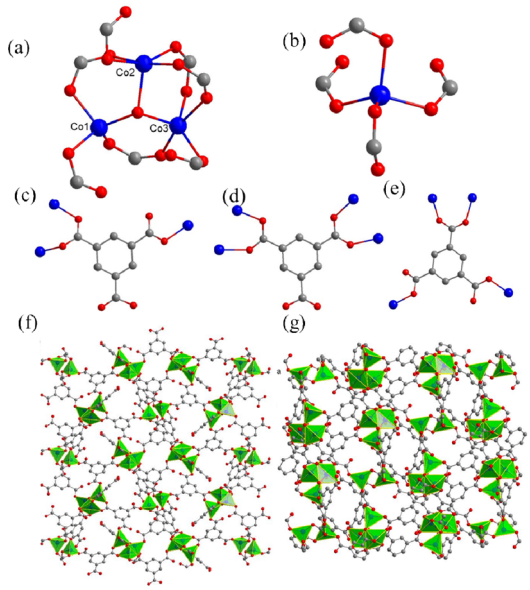

Figure 1. (a) SBU coordination environment of trimeric $[Co_3(\mu_3\text{-}OH)(COO)_7]$ SBU units in **NTU-Z30**. (b) Second mononuclear $[Co(COO)_4]$ SBU units in **NTU-Z30**. (c–e) Coordination of the BTC ligand. (f) Bar-and-stick model of **NTU-Z30** along the *a* axis. (g) Bar-and-stick model of **NTU-Z30** viewed along the *b* axis. (Note that H atoms and all guest molecules have been omitted for clarity. Color code: Co, blue; O, red; C, gray.)

COO groups and one μ_3-OH (Figure 1a). In this new trimeric SBU, two Co^{2+} centers (Co2 and Co3) display a trigonal-bipyramidal configuration and coordinate with one μ_3-OH (Co–O 1.9723–2.1390 Å, Co3–μ_3-OH 2.0526 Å, and Co2–μ_3-OH 2.0768 Å) and four different O species from different COO units, while the third Co^{2+} center (Co1) is four-connected with one μ_3-OH (Co–O 1.9633–1.9957 Å) and three different O atoms from different COO units. The second SBU (Figure 1b) is a mononuclear $[Co(COO)_4]$ species that is constructed by one Co^{2+} center and four O atoms from four different COO units with monodentate coordination mode (Co–O 1.9520–1.9874 Å). The ratio between these two SBUs in **NTU-Z30** is 1:1. Moreover, there are three independent BTC linkers in **NTU-Z30**: one BTC is linked with Co cations through two different –COO groups with one bridging μ_2-η^1:η^1 mode and a monodentate η^1 mode (Figure 1c), the second one has two bridging μ_2-η^1:η^1 modes (Figure 1d), and the third one has one bridging μ_2-η^1:η^1 mode and two monodentate η^1 modes (Figure 1e). The two SBUs are further linked together through BTC units to form three-dimensional structures with an intercrossed channel along the *a* and *b* axes (Figure 1f,g). Protonated $HTEA^+$ and guest H_3O^+ cations act as charge-balance species and fill up the empty space in the channels. TGA (Figure S3, SI) for **NTU-Z30** reveals that the weight loss (22.85%) in the first stage between 80 and 375 °C is attributed to the loss of TEA and H_2O (calcd 23.30%), and the weight loss of 64.35% in the second stage between 375 and 600 °C can be explained by the loss of BTC linkers (calcd 63.74%). The final residue of 12.80% is close to the calculated amount of CoO (12.96%; Figure S3, SI).

Structure Description of NTU-Z31. As shown in Figure 2a, a three-dimensional structure of **NTU-Z31** is made from dimeric cobalt carboxylate clusters and BTC linkers[8f]. In $Co_2(COO)_6$ clusters, one Co atom has an inversion center symmetry to the other. Each Co center has a distorted tetrahedral geometry (Co–O 1.9488–2.0048 Å) and coordinates with four O atoms from four different but symmetrically equivalent BTC ligands through a bridging μ_2-η^1:η^1 mode and two monodentate η^1 modes (Figure 2b), resulting in a three-dimensional network (Figure 2c). As shown in Figure 2d, the framework of **NTU-Z31** can be viewed as a decorated rutile net, where each BTC ligand links to three different SBUs and each SBU connects to six BTC ligands. The guest H_2O and guest $HTEA^+$ occupy the vacancies made by asymmetric units and have strong interaction with the network via hydrogen bonds. The weight loss of 28.35% (first stage) between 150 and 260 °C in TGA is attributed to the loss of guest TEA and H_2O (calcd 27.03%), and the weight loss of 54.26% in the second

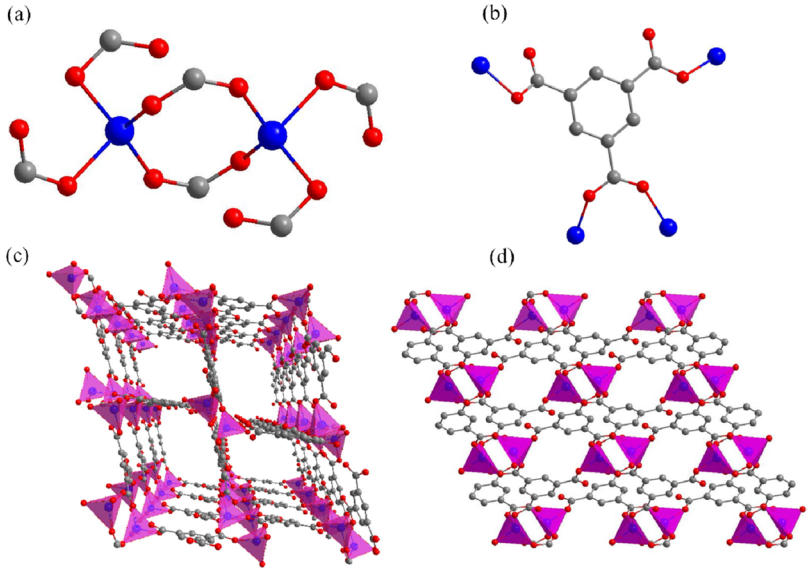

Figure 2. (a) SBU coordination environment of the dimeric cobalt units in **NTU-Z31**. (b) Coordination of the BTC ligand. (c) Bar-and-stick model for **NTU-Z31** viewed along the *a* axis. (d) Bar-and-stick model for **NTU-Z31** along the *b* axis (H atoms, H_2O, and HTEA have been omitted for clarity. Color code: Co, blue; C, gray; O, red.)

dx.doi.org/10.1021/ic5011133 | *Inorg. Chem.* 2014, 53, 8529–8537

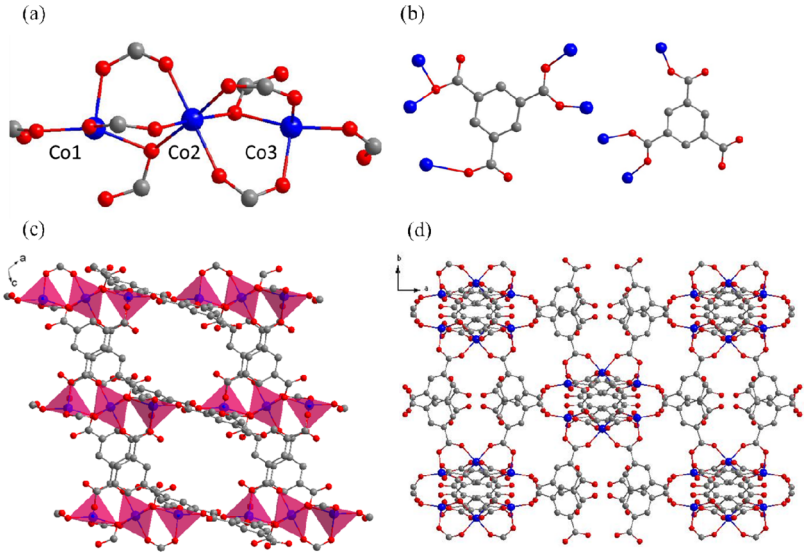

Figure 3. (a) SBU coordination environment of trinuclear cobalt units in **NTU-Z32**. (b) Coordination of the BTC ligand. (c) Bar-and-stick model of **NTU-Z32** viewed along the *b* axis. (d) Bar-and-stick model for **NTU-Z32** viewed along the *c* axis. (H atoms and HTEA molecules have been omitted for clarity. Color code: Co, blue; C, gray; O, red.)

stage from 260 to 700 °C corresponds to the loss of BTC linkers (calcd 55.40%). The final residue of 17.57% is close to the calculated amount of CoO (17.39%; see Figure S3, SI).

Structure Description of NTU-Z32. The three-dimensional framework of **NTU-Z32** is constructed by BTC ligands and trinuclear $[Co_3(COO)_8]^{2-}$ SBUs. As shown in Figure 3a, the linear Co_3 SBU consists of three crystallographically independent Co centers (Co1, Co2, and Co3). The central Co atom (Co2) has an octahedral configuration with all bridging −COO species from six different BTC ligands, while the terminal centers Co1 and Co3 adopt a four-coordinated distorted tetrahedron, which is completed by bridging four −COO groups from three different BTC ligands. The lengths of the Co−O bonds are in the range of 1.9452−2.1642 Å. The Co1−Co2−Co3 angle is ca. 144.556° (30), and the distances between metal centers are about 3.3969(11) Å. In addition, two independent BTC linkers are observed in **NTU-Z32**: one BTC is linked to Co centers via −COO groups through μ_2-η^2 mode, μ_2-η^1:η^1 mode, and monodentate η^1 mode (Figure 3b), and the second one has μ_2-η^1:η^1 mode and η^1 mode (Figure 3b). The framework of **NTU-Z32** has channels with a diameter of ~12.56 Å along the *b* axis, where $HTEA^+$ cations were filled for charge balance (Figure 3c). In **NTU-Z32**, each Co_3 SBU connects with eight BTC ligands, and every BTC ligand links two or three Co_3 SBUs, leading to the formation of a three-dimensional framework (Figure 3d). Noting that **NTU-Z32** is an analogue of $Ni_3(NMe_4)(BTC)_3(DMF)_2$ except the coordination environments of metal atoms.[8d,e,18] TGA for **NTU-Z32** (Figures S3, SI) shows that the weight loss (20.05%) in the first stage (150−300 °C) belongs to the evaporation of guest TEA (calcd 20.28%), and the weight loss (59.58%) in the second stage (300−600 °C) comes from the loss of coordination BTC ligands (calcd 57.06%). The final residue of 21.37% is close to the calculated amount of CoO (22.66%; Figure S3, SI).

Topology Studies. The net topologies of **NTU-Z30**, **NTU-Z31**, and **NTU-Z32** have been studied. Considering SBUs $[Co_3(\mu_3\text{-}OH)(COO)_7]$ and $[Co(COO)_4]$ in **NTU-Z30** as nodes, **NTU-Z30** can be simplified as a novel 3,3,6,7-c net with stoichiometry (3-c)2(3-c)2(6-c)(7-c)2 (4-nodal net; Figure 4a), and the point symbol for the net is {4^2.5^4.6^7.8.9}{4^2.5}2{4^3.5^6.6^10.7.8}2{5.6^2}2. Similarly, **NTU-Z31** will have a known topology type **rtl** *rutile* (3,6-c net with stoichiometry (3-c)2(6-c); 2-nodal net) with a point symbol for the net of {4.6^2}2{4^2.6^10.8^3} (Figure 4b). **NTU-Z32** will possess a novel topology 2,8-c net with stoichiometry (2-c)4(8-c) (2-nodal net; Figure 4c), and the point symbol for net is {4^4.12^24}{4}4, while the point symbol for the net with loops is {2^4.6^24}{2}4. All topology nets are viewed along the *b* axis. The views from other directions (*a* and *c* axes) are provided in the SI (Figure S8). The topology study clearly indicates that, under similar synthetic conduction, the ratio of metal and linkers has a big effect on their structures.

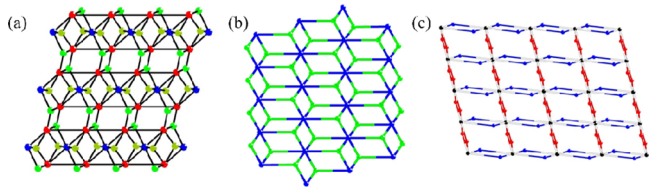

Figure 4. Simplified topologies of **NTU-Z30** (a), **NTU-Z31** (b), and **NTU-Z32** (c) viewed along the *b* axis.

Magnetic Properties. The magnetic properties of **NTU-Z30** (a), **NTU-Z31** (b), and **NTU-Z32** (c) have been examined for possible applications as molecular magnets.[6d] The magnetic susceptibilities (χ_M) of all samples were tested from 300 to 2 K under 100 Oe (Figure 5), and χ_M of all materials follows the Curie−Weiss law in the testing temperature range. The calculated Curie (*C*) and Weiss (θ) constants for **NTU-Z30**, **NTU-Z31**, and **NTU-Z32** are 3.10 cm^3 K mol^{-1} and −33.50 K, 2.92 cm^3 K mol^{-1} and −24.51 K, and 2.34 cm^3 K mol^{-1} and −33.10 K, respectively. These results suggest that the neighboring Co cations in all three MOFs have weak antiferromagnetic interactions.

Catalytic Activity of NTU-Z30. Except for the synthesis of novel MOF materials, the efforts are also invested on their possible applications in many fields. Among the recent development, MOFs as effective heterogeneous catalysts have

dx.doi.org/10.1021/ic5011133 | Inorg. Chem. 2014, 53, 8529−8537

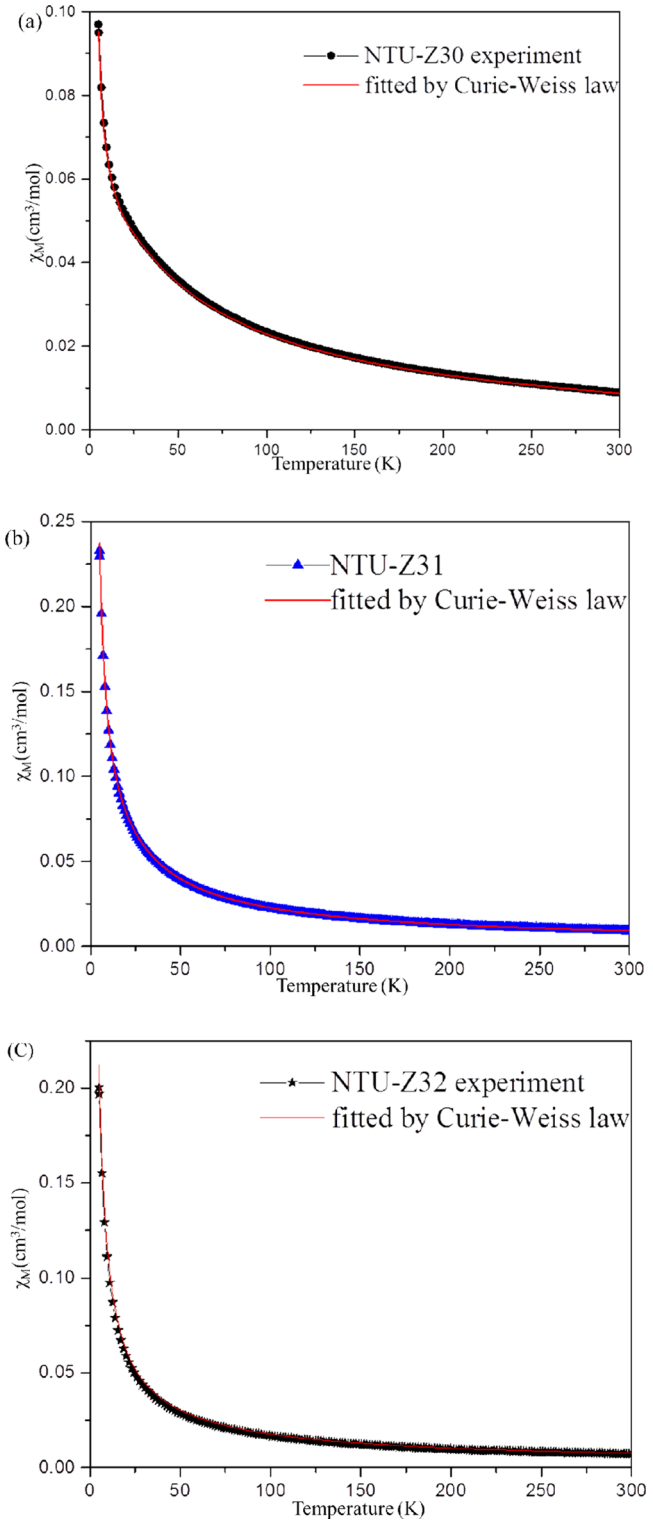

Figure 5. Temperature dependence of magnetic susceptibilities of **NTU-Z30** (a), **NTU-Z31** (b), and **NTU-Z32** (c).

been comprehensively investigated especially in the epoxidation of alkenes.[20] Herein, the catalytic activity of the synthesized MOFs was performed using O_2 gas to oxide *trans*-stilbene into epoxides with DMF as reaction media.

Although they could show some certain catalytic activities, **NTU-Z31** and **NTU-Z32** are unstable in DMF and are screened out for catalytic examination. The stable **NTU-Z30** is the main object to be examined on the catalytic activity in the aerobic epoxidation as below. Figure 6 displays the relationship

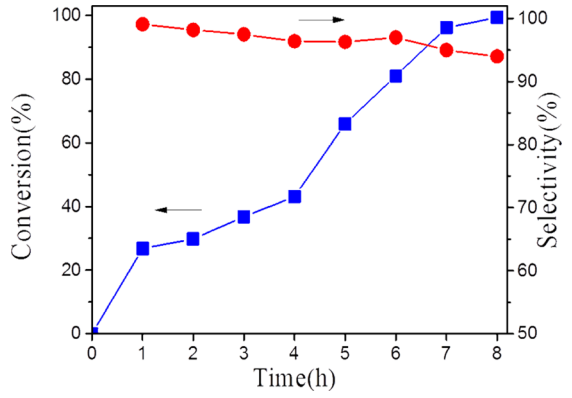

Figure 6. NTU-Z30-catalyzed epoxidation of *trans*-stilbene. Reaction conditions: *trans*-stilbene, 1 mmol; **NTU-Z30**, 2.5 mg; DMF, 15 mL; flow rate of O_2, 30 mL min^{-1}; reaction temperature, 100 °C.

between the time and epoxidation ratio of *trans*-stilbene, where the conversion (98.2%) and selectivity (95.6%) toward the epoxide can be observed after 7 h of reaction. The average turnover frequency (TOF) of 17.6 h^{-1} based on the cobalt mass was obtained for a reaction lasting for 6 h at 100 °C with an O_2 flow rate of 30 mL min^{-1}. Elevating the reaction temperature or O_2 flow rate could further improve the average TOFs (TOF = 20.5 h^{-1} when the reaction temperature is 120 °C). The catalytic activity of **NTU-Z30** has been compared with the reported representative catalysts for the same reaction, and the results are summarized in Table 1. For transformation

Table 1. Epoxidation of *trans*-Stilbene Catalyzed by a Series of Catalysts[20]

catalyst	conversion (%)	selectivity (%)	TOF[a] (h^{-1})	ref
$[Mn(\mu\text{-terph})(H_2O)_2]_n$		<7		19
PW_x/MIL-101	35	69	6.6	4f
$[Co(Hoba)_2]$	86	100		18h
STA-12(Co)	95	89	11.7	18i
NTU-Z30[a]	96.2	98.6	17.6	this work

[a]Reaction conditions: *trans*-stilbene, 1 mmol; **NTU-Z30**, 2.5 mg; solvent, 15 mL; O_2 flow speed, 30 mL min^{-1}; reaction duration, 7 h; reaction temperature, 100 °C.

from *trans*-stilbene to its corresponding epoxide, **NTU-Z30** shows high epoxide selectivity, excellent conversion ratio, and high TOF value, surpassing most of the reported MOF-based heterogeneous catalysts for the same reaction,[18h,i] and even rivals some traditional catalysts.[20] Note that most reports involving MOF-based catalysts have to involve either cocatalyst or peroxides because of their poor catalytic behaviors. Clearly, the **NTU-Z30** catalyst takes the lead among all MOF-based catalysts to approach a good catalytic performance.

To optimize the reaction conditions, a series of control experiments with different reaction parameters were performed (Figure 7). Clearly, the reaction rate is increased with increasing temperature (Figure 7a). For example, a lower conversion (39.7%) was observed when the reaction was performed at 80 °C. If the reaction temperature was raised to 120 °C, a higher conversion (larger than 96.1%) was achieved.

dx.doi.org/10.1021/ic5011133 | Inorg. Chem. 2014, 53, 8529−8537

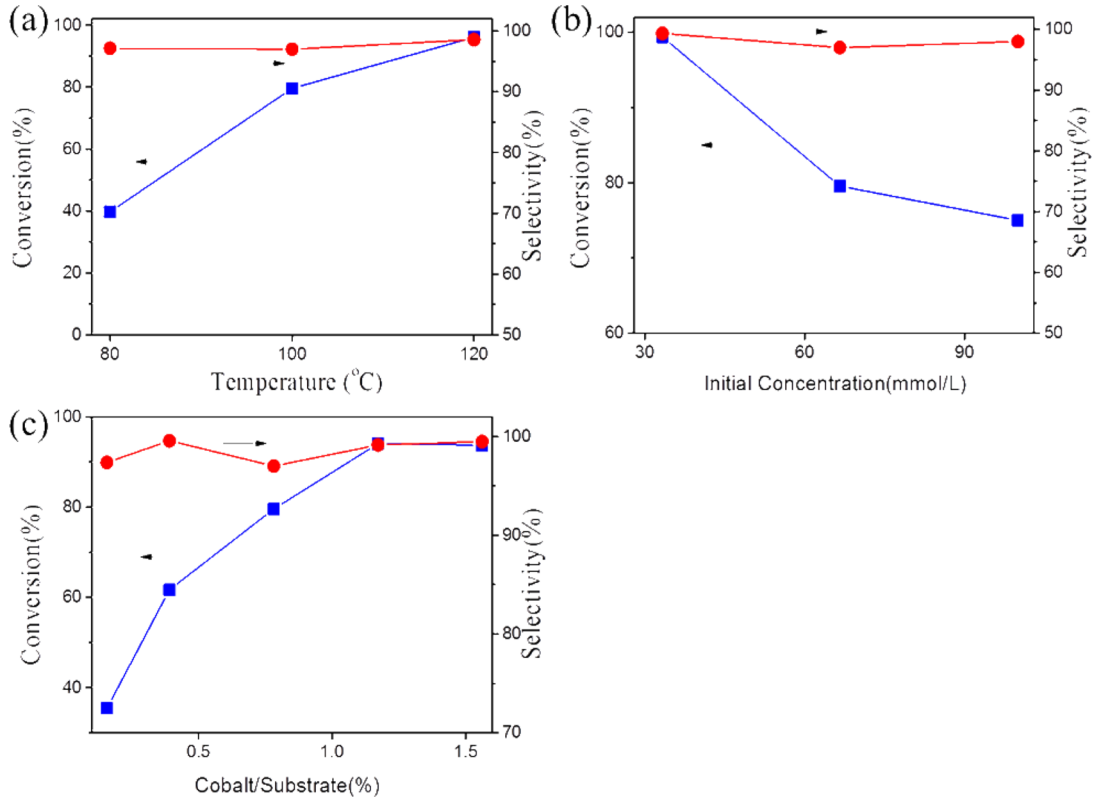

Figure 7. Effect of several reaction parameters for aerobic epoxidation of *trans*-stilbene: (a) effect of the reaction temperature; (b) effect of the catalyst amount; (c) effect of the initial concentration. The reaction duration is 6 h, and the other reaction parameters are similar to those in Figure 6.

In the whole temperature range, the selectivity remains at a high value over 97.0%, showing no obvious correlation with the temperature change. In addition, the reaction rate was strongly affected by the O_2 flow rate. For example, the conversion increases as the amount of catalyst (Figure 7b) increases up to 3.75 mg, suggesting that the reaction rate might not be majorly limited by the mass-transfer effect. Moreover, the concentration effect of the initial substrates was also observed through adjustment of the volume of the solvent but maintaining a constant ratio of cobalt/substrate. As shown in Figure 7c, a higher conversion could be observed within some ranges of higher initial concentrations.

In fact, the solvent has an important role in the oxidation of *trans*-stilbene. For example, when this type of reaction was performed in dimethyl sulfoxide (DMSO) and 1,2-dichlorobenzene (ODCB), no epoxidation compounds were formed. However, when cyclohexanone and *N*,*N*-dimethylacetamide (DMA) were employed as reaction media, epoxidation products with high reaction rate were observed (Table 2). In fact, the aerobic epoxidations only process well in some selected solvents, especially alkylamide solvents. Several reports have already demonstrated that DMF is a good solvent for the successful aerobic epoxidation of alkenes with the heterogeneous cobalt catalyst in the absence of additional radical initiators or sacrificial reductants.[18,19] The use of amide solvents (e.g., DMF) is necessary for the Co-DMF complex to show the decent catalytic activity because the Co-DMF complex might react with O_2 molecules to form a cobalt superoxo species capable of transferring the oxygen to the alkene.[20]

Table 2. Solvent Effect on NTU-Z30-Catalyzed Reactions[a]

entry	substrate	conversion (%)	selectivity (%)
1	DMF	79.6	97.0
2	DMSO		
3	ODCB		
4	DMA	98.2	36.1
5	cyclohexanone	95.8	88.2

[a]Reaction conditions: *trans*-stilbene, 1 mmol; **NTU-Z30**, 2.5 mg; solvent, 15 mL; O_2 flow speed, 30 mL min^{-1}; reaction temperature, 100 °C; reaction duration, 6 h.

On the other hand, the high reactivity of DMF with oxygen might support the unusual solvent effect. It is found that, even under relatively mild conditions, DMF can be autoxidized by O_2 molecules to form *N*-(hydroperoxymethyl)-*N*-methylformamide, which is an important intermediate to transfer the O_2 to the substrate.[19,21] Therefore, it should not be surprising to investigate that *trans*-stilbene still can be converted into the corresponding epoxide under the same reaction conditions, even the reaction system did not have any catalysts.

Besides *trans*-stilbene, **NTU-Z30** has also been demonstrated to show quite good catalytic epoxidation to other alkenes (Table 3), no matter the rigid structure and weak nucleophilicity (*cis*-cyclooctene, entry 4) or the alphalic alkene (1-decene, entry 5). The results strongly support that the good ability of **NTU-Z30** to catalyze aerobic epoxidation reaction should have the potential for application in epoxidation industries.

Stability of NTU-Z30. If considering a similar mechanism of the metal ion embedded in a MOF similar to the homogeneous cobalt catalyst, the structure of the MOF should not only allow expansion of the metal ion's coordination sphere but also a change of valence. However, this process may cause metal leaching, leading to the appearance of an issue, if the

dx.doi.org/10.1021/ic5011133 | *Inorg. Chem.* 2014, 53, 8529−8537

Table 3. Epoxidized Behaviors of Various Alkenes over NTU-Z30[a]

entry	substrate	conversion (%)	selectivity[b] (%)	turnover number[c]
1	*trans*-stilbene	79.6	97.0	101.9
3	styrene	99.1	37.4	126.8
4	*cis*-cyclooctene	16.5	97.5	21.1
5	1-decene	10.3	82.7	13.2
6	*trans*-stilbene[d]	0.27	100.0	0.34

[a]Reaction conditions: substrate, 1 mmol; **NTU-Z30**, 2.5 mg; solvent, DMF, 15 mL; O_2 flow speed, 30 mL min^{-1}; temperature, 100 °C; reaction duration, 6 h. [b]The selectivity to corresponding epoxides for each starting compound: byproduct benzaldehyde for *trans*-stilbene; byproducts benzoic acid and benzaldehyde for styrene; byproducts 4-cyclooctene-1-one and 2-cyclooctene-1-one for *cis*-cyclooctene; byproduct 3-decanone for 1-decene. [c]TON was calculated by millimoles of starting compounds changed to corresponding epoxides/mmol of Co ions in **NTU-Z30**. [d]0.01 mmol of BHT was used the radical scavenger.

catalysis proceeds mainly heterogeneously with MOF as the solid catalyst, concerning the stability of the MOF during the reaction.[22]

In this work, examination of the nature of catalysis by hot filtration was performed, which is a routine control experiment for works with the MOF as a heterogeneous catalyst.[2e] As shown in Figure 8, when the reaction proceeded after removal

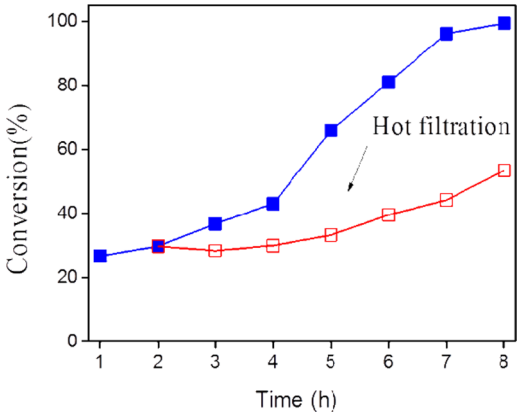

Figure 8. Comparison of the epoxidation of *trans*-stilbene without catalyst removal after 2 h (the reaction parameters are similar to those in the footnote of Figure 6).

of **NTU-Z30**, an obviously reduced reaction rate was observed. Leaching analysis after 6 h of reaction shows that the leaching cobalt amount in the liquid is negligible compared to approximately 0.3% of the employed cobalt in the whole reaction, which reasonably supports that the excellent catalytic behavior mainly comes from the heterogeneous route.

The stability of **NTU-Z30** has been carefully investigated because it is an important factor in evaluating the heterogeneous catalyst. The recycle experiments of **NTU-Z30** were performed, and the results are summarized in Figure 9. Surprisingly, after the first run, the recycled **NTU-Z30** showed an even greater catalytic activity. In the second run, the conversion and selectivity of *trans*-stilbene toward epoxide reaches 92.5% and 99.3%, respectively. After the third run, the conversion got increased to 97.4% and the selectivity is 98.6%. According to the calculation from *Diamond* software, the larger

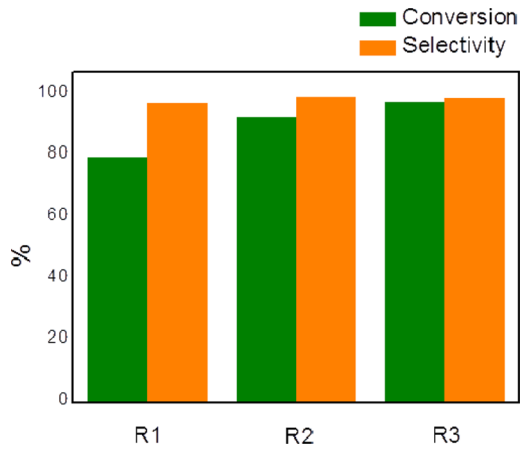

Figure 9. Recycle experiment of **NTU-Z30** for epoxidation of *trans*-stilbene.

pore size of **NTU-Z30** is 12 × 10 Å along the *a* axis; hence, the molecule as large as *trans*-stilbene is unable to enter the pore and contact with the active cobalt sites inside. Here we attribute the active cobalt sites to the cobalt sites on the outer surface of **NTU-Z30**. Therefore, the improved catalytic activity in the recycle test infers that **NTU-Z30** turns to fragments to some extent and then a larger surface area is exposed or rather the number of active sites increases, which leads to the improved catalytic activity. The catalyst stability was further examined by PXRD and FTIR spectra. The PXRD (Figure S5, SI) study of both pristine and spent **NTU-Z30** shows no phase change, while no obvious peak shifts in the FTIR spectra (Figure S6, SI) further confirm the stability of **NTU-Z30**, which is in agreement with the result of recycle usage. However, according to the ICP-MS result, only a negligible amount of cobalt species leaches into the solution, which might be due to expansion of the cobalt coordination sphere or removal of the cobalt ion, causing the collapse of the framework.

In order to understand the epoxidation mechanism catalyzed by **NTU-Z30**, a tiny amount of butylhydroxytoluene (BHT; free radical scavenger) was added into the reaction and a "zero" conversion of *trans*-stilbene was observed (Table 3), indicating that Co-MOF-catalyzed epoxidation should involve radical species.[22]

In fact, many Co^{2+} complexes have been demonstrated to show the ability to coordinate with O_2 molecules and activate it to produce a complicated intermediate [e.g., $Co^{3+}(O^{2-})$].[23] Therefore, we believe that a similar attachment of O_2 to Co^{2+} centers could also happen in the initial step. The in situ generated intermediate $Co^{3+}(O^{2-})$ pieces might produce an active radical oxygen species to complete the epoxidation reaction. To understand the catalytic process more thoroughly, UV−vis absorption spectroscopy has been employed to characterize the pristine **NTU-Z30** and the spent one (Figure 10). The UV−vis absorption spectrum of the pristine **NTU-Z30** shows ambiguous bands in a broad range of 380−680 nm. The shoulder peaks at 491 and 533 nm assigned to the $^4A_2 \rightarrow {}^4E$ (P) transition are attributed to Co^{2+} in trigonal-bipyramidal sites. The weak bands (560−610 nm) are attributed to Co^{2+} in pseudotetrahedral sites due to the $^4A_2 \rightarrow {}^4T_1$ (P) transition.[24] The coordination environment of cobalt sites indicated by the UV−vis result of the pristine **NTU-Z30** is in agreement with that determined through single-crystal structure analysis: Co^{2+} is tetrahedrally and trigonal-bipyramidally coordinated by BTC

dx.doi.org/10.1021/ic5011133 | *Inorg. Chem.* 2014, 53, 8529−8537

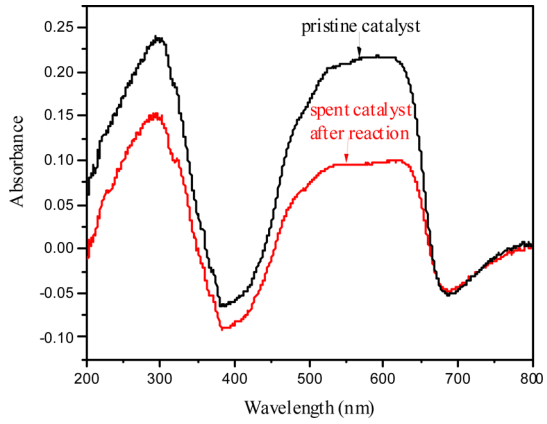

Figure 10. UV−vis spectra of **NTU-Z30** for the epoxidation of *trans*-stilbene.

links. The Co ion as the active site embedded in the framework normally undergoes a one-electron redox change in a typical cycle during the catalytic process, while the challenge appears then to keep the Co ion well fixed in the lattice in the oxidation state.

For contrast, in the spectrum of the spent **NTU-Z30**, an obvious change was not observed, which indicates that the majority of the cobalt species are divalent. This suggests that the proposed Co^{3+}-OOR intermediate has a strong tendency to revert to the divalent state, which guarantees that the cobalt is in the lattice. This agrees on the excellent stability during the reaction. Nevertheless, more researches are required to provide enough evidence for the postulated intermediates.

CONCLUSION

In short, three novel three-dimensional Co-MOFs have been successfully prepared under surfactant-thermal conditions, and their structures have been determined by single-crystal analysis. The topology studies reveal that **NTU-Z30** and **NTU-Z32** possess two new topologies: 3,3,6,7-c net and 2,8-c net, respectively. Magnetic studies of all three MOFs indicate that all materials display weak antiferromagnetic behaviors. Among all catalytic epoxidations of *trans*-stilbene, the catalytic activity of **NTU-Z30** takes advantage of all reported similar MOF materials. In addition, **NTU-Z30** also has high selectivity, excellent conversion, and high TOF values among all reported MOF-based catalysts. Our success in employing surfactants as reaction media to prepare novel MOFs with various structures could be a promising strategy to approach other crystalline inorganic materials.

ASSOCIATED CONTENT

Supporting Information

Photographs of crystals, tables of different synthetic conditions to prepare MOFs and of crystal and structure refinement data, PXRD pattern, TGA analysis, FTIR spectra, thermal ellipsoid plots of all MOFs, net topologies, and CIF files. This material is available free of charge via the Internet at http://pubs.acs.org.

AUTHOR INFORMATION

Corresponding Authors

*E-mail: yhyang@ntu.edu.sg.
*E-mail: bygeng@mail.ahnu.edu.cn.
*E-mail: qczhang@ntu.edu.sg.

Author Contributions

§Both authors have equal contribution to this paper.

Notes

The authors declare no competing financial interest.

ACKNOWLEDGMENTS

The authors thank Prof. Tao Wu and Jian Lin for topology analysis. Q.Z. acknowledges AcRF Tier 1 (RG 16/12) and Tier 2 (ARC 2/13 and ARC 20/12) from MOE and the CREATE program (Nanomaterials for Energy and Water Management) from NRF Singapore. This work was also supported by the National Natural Science Foundation of China (Grant 21271009).

REFERENCES

(1) (a) Brown, J. W.; Henderson, B. L.; Kiesz, M. D.; Whalley, A. C.; Morris, W.; Grunder, S.; Deng, H.; Furukawa, H.; Zink, J. I.; Stoddart, J. F.; Yaghi, O. M. *Chem. Sci.* **2013**, *4*, 2858. (b) Furukawa, H.; Cordova, K. E.; O'Keeffe, M.; Yaghi, O. M. *Science* **2013**, *341*, 1230444. (c) Li, J. R.; Kuppler, R. J.; Zhou, H. C. *Chem. Soc. Rev.* **2009**, *38*, 1477. (d) Zheng, S.; Bu, J. T.; Li, Y.; Wu, T.; Zuo, F.; Feng, P.; Bu, X. *J. Am. Chem. Soc.* **2010**, *132*, 17062. (e) Gao, J.; Ye, K.; He, M.; Cao, W.; Xiong, W. W.; Lee, Z. Y.; Wang, Y.; Wu, T.; Huo, F.; Liu, X.; Zhang, Q. *J. Solid State Chem.* **2013**, *206*, 27. (f) Gao, J.; Ye, K.; Yang, L.; Xiong, W. W.; Ye, L.; Wang, Y.; Zhang, Q. *Inorg. Chem.* **2014**, *53*, 691. (g) Cui, Y. J.; Yue, Y. F.; Qian, G. D.; Chen, B. L. *Chem. Rev.* **2012**, *112*, 1126. (h) Wang, F.; Liu, Z. S.; Yang, H.; Tan, Y. Z.; Zhang, J. *Angew. Chem., Int. Ed.* **2011**, *50*, 450. (i) Nguyen, D.-T.; Chew, E.; Zhang, Q.; Choi, A.; Bu, X. *Inorg. Chem.* **2006**, *45*, 10722.

(2) (a) Yang, Q.; Guillerm, V.; Ragon, F.; Wiersum, A. D.; Llewellyn, P. L.; Zhong, C.; Devic, T.; Serre, C.; Maurin, G. *Chem. Commun.* **2012**, *48*, 9831. (b) Gong, Y. N.; Meng, M.; Zhong, D. C.; Huang, Y. L.; Jiang, L.; Lu, T. B. *Chem. Commun.* **2012**, *48*, 12002. (c) Volkringer, C.; Popov, D.; Loiseau, T.; Guillou, N.; Ferey, G.; Haouas, M.; Taulelle, F.; Mellot-Draznieks, C.; Burghammer, M.; Riekel, C. *Nat. Mater.* **2007**, *6*, 760−4. (d) Gao, J.; Maio, J.; Li, P.-Z.; Teng, W. Y.; Yang, L.; Zhao, Y.; Liu, B.; Zhang, Q. *Chem. Commun.* **2014**, *50*, 3786. (e) Gao, J.; Bai, L.; Zhang, Q.; Li, Y.; Rakesh, G.; Lee, J.-M.; Yang, Y.; Zhang, Q. *Dalton Trans.* **2014**, *43*, 2559. (f) Wang, C.; DeKrafft, K. E.; Lin, W. *J. Am. Chem. Soc.* **2012**, *134*, 7211. (g) Xiong, W. W.; Zhang, G.; Zhang, Q. *Inorg. Chem. Frontiers* **2014**, *1*, 292.

(3) (a) Dang, S.; Min, X.; Yang, W.; Yi, F. Y.; You, H.; Sun, Z. M. *Chem.—Eur. J.* **2013**, *19*, 17172. (b) Yu, J.; Cui, Y.; Wu, C.; Yang, Y.; Wang, Z.; O'Keeffe, M.; Chen, B.; Qian, G. *Angew. Chem., Int. Ed.* **2012**, *51*, 10542. (c) Wang, C.; Zhang, T.; Lin, W. *Chem. Rev.* **2012**, *112*, 1084. (d) Huang, Q.; Yu, J.; Gao, J.; Rao, X.; Yang, X.; Cui, Y.; Wu, C.; Zhang, Z.; Xiang, S.; Chen, B.; Qian, G. *Cryst. Growth Des.* **2010**, *10*, 5291.

(4) (a) Katz, M. J.; Mondloch, J. E.; Totten, R. K.; Park, J. K.; Nguyen, S. T.; Farha, O. K.; Hupp, J. T. *Angew. Chem., Int. Ed.* **2014**, *53*, 497. (b) Platero-Prats, A. E.; Snejko, N.; Iglesias, M.; Monge, A.; Gutierrez-Puebla, E. *Chem.—Eur. J.* **2013**, *19*, 15572. (c) Juan-Alcañiz, J.; Ferrando-Soria, J.; Luz, I.; Serra-Crespo, P.; Skupien, E.; Santos, V. P.; Pardo, E.; Llabrés i Xamena, F. X.; Kapteijn, F.; Gascon, J. *J. Catal.* **2013**, *307*, 295. (d) Park, J.; Li, J. R.; Chen, Y. P.; Yu, J.; Yakovenko, A. A.; Wang, Z. U.; Sun, L. B.; Balbuena, P. B.; Zhou, H. C. *Chem. Commun.* **2012**, *48*, 9995. (e) Paz, F. A.; Klinowski, J.; Vilela, S. M.; Tome, J. P.; Cavaleiro, J. A.; Rocha, J. *Chem. Soc. Rev.* **2012**, *41*, 1088. (f) Maksimchuk, N. V.; Kovalenko, K. A.; Arzumanov, S. S.; Chesalov, Y. A.; Melgunov, M. S.; Stepanov, A. G.; Fedin, V. P.; Kholdeeva, O. A. *Inorg. Chem.* **2010**, *49*, 2920.

(5) (a) Talin, A. A.; Centrone, A.; Ford, A. C.; Foster, M. E.; Stavila, V.; Haney, P.; Kinney, R. A.; Szalai, V.; El Gabaly, F.; Yoon, H. P.; Leonard, F.; Allendorf, M. D. *Science* **2014**, *343*, 66. (b) Kreno, L. E.; Leong, K.; Farha, O. K.; Allendorf, M.; Van Duyne, R. P.; Hupp, J. T. *Chem. Rev.* **2012**, *112*, 1105. (c) Li, M.; Dinca, M. *J. Am. Chem. Soc.* **2011**, *133*, 12926.

(6) (a) Deng, Y.; Wei, J.; Sun, Z.; Zhao, D. *Chem. Soc. Rev.* **2013**, *42*, 4054. (b) Sun, L. B.; Yang, J.; Kou, J. H.; Gu, F. N.; Chun, Y.; Wang, Y.; Zhu, J. H.; Zou, Z. G. *Angew. Chem., Int. Ed.* **2008**, *47*, 3418. (c) Sun, L. B.; Tian, W. H.; Liu, X. Q. *J. Phys. Chem. C* **2009**, *113*, 19172. (d) Kurmoo, M. *Chem. Soc. Rev.* **2009**, *38*, 1353.

(7) (a) Cao, L.; Tao, J.; Gao, Q.; Liu, T.; Xia, Z.; Li, D. *Chem. Commun.* **2014**, *50*, 1665. (b) Pullen, S.; Fei, H.; Orthaber, A.; Cohen, S. M.; Ott, S. *J. Am. Chem. Soc.* **2013**, *135*, 16997.

(8) (a) Cai, J.; Rao, X.; He, Y.; Yu, J.; Wu, C.; Zhou, W.; Yildirim, T.; Chen, B.; Qian, G. *Chem. Commun.* **2014**, *50*, 1552. (b) Reinsch, H.; Kruger, M.; Marrot, J.; Stock, N. *Inorg. Chem.* **2013**, *52*, 1854. (c) Jeong, S.; Song, X.; Jeong, S.; Oh, M.; Liu, X.; Kim, D.; Moon, D.; Lah, M. S. *Inorg. Chem.* **2011**, *50*, 12133. (d) Du, Y.; Thompson, A. L.; Russell, N.; O'Hare, D. *Dalton Trans.* **2010**, *39*, 3384. (e) Du, Y.; Thompson, A. L.; O'Hare, D. *Chem. Commun.* **2008**, 5987. (f) Xie, L.; Liu, S.; Gao, B.; Zhang, C.; Sun, C.; Li, D.; Su, Z. *Chem. Commun.* **2005**, 2402.

(9) (a) Cameron, J. M.; Gao, J.; Vila-Nadal, L.; Long, D. L.; Cronin, L.; Formation. *Chem. Commun.* **2014**, *50*, 2155. (b) Tonigold, M.; Lu, Y.; Mavrandonakis, A.; Puls, A.; Staudt, R.; Mollmer, J.; Sauer, J.; Volkmer, D. *Chem.—Eur. J.* **2011**, *17*, 8671.

(10) (a) Kang, Y.; Chen, S.; Wang, F.; Zhang, J.; Bu, X. *Chem. Commun.* **2011**, *47*, 4950. (b) Zhang, J.; Bu, J. T.; Chen, S.; Wu, T.; Zheng, S.; Chen, Y.; Nieto, R. A.; Feng, P.; Bu, X. *Angew. Chem., Int. Ed.* **2010**, *49*, 8876.

(11) (a) Gao, J.; Tay, Q.; Li, P. Z.; Xiong, W. W.; Zhao, Y.; Chen, Z.; Zhang, Q. *Chem.—Asian J.* **2014**, *9*, 131. (b) Shang, W.; Kang, X.; Ning, H.; Zhang, J.; Zhang, X.; Wu, Z.; Mo, G.; Xing, X.; Han, B. *Langmuir* **2013**, *29*, 13168. (c) Sun, L. B.; Li, J. R.; Park, J.; Zhou, H. C. *J. Am. Chem. Soc.* **2012**, *134*, 126. (d) Guo, Y.-N.; Li, Y.; Zhi, B.; Zhang, D.; Liu, Y.; Huo, Q. *RSC Adv.* **2012**, *2*, 5424. (e) Lin, H.; Zhu, G.; Xing, J.; Gao, B.; Qiu, S. *Langmuir* **2009**, *25*, 10159. (f) Lu, G.; Li, S. Z.; Guo, Z.; Farha, O. K.; Hauser, B. G.; Qi, X. Y.; Wang, Y.; Wang, X.; Han, S. Y.; Liu, X. G.; DuChene, J. S.; Zhang, H.; Zhang, Q.; Chen, X. D.; Ma, J.; Loo, S. C. J.; Wei, W. D.; Yang, Y. H.; Hupp, J. T.; Huo, F. W. *Nat. Chem.* **2012**, *4*, 310. (g) Liu, Y.; Boey, F.; Lao, L. L.; Zhang, H.; Liu, X.; Zhang, Q. *Chem.—Asian J.* **2011**, *6*, 1004. (h) Xiao, J.; Yin, Z.; Wu, Y.; Guo, J.; Cheng, Y.; Li, H.; Huang, Y. Z.; Zhang, Q.; Ma, J.; Boey, F.; Zhang, H.; Zhang, Q. *Small* **2011**, *7*, 1242. (i) Lin, Z. Q.; Sun, P.-J.; Tay, Y. Y.; Liang, J.; Liu, Y.; Shi, N.-E.; Xie, L.-H.; Yi, M.-D.; Qian, Y.; Fan, Q.-L.; Zhang, H.; Hng, H. H.; Ma, J.; Zhang, Q.; Huang, W. *ACS Nano* **2012**, *6*, 5309.

(12) (a) Xiong, W. W.; Athresh, E. U.; Ng, Y. T.; Ding, J.; Wu, T.; Zhang, Q. *J. Am. Chem. Soc.* **2013**, *135*, 1256. (b) Xiong, W. W.; Miao, J.; Li, P.-Z.; Zhao, Y.; Liu, B.; Zhang, Q. *CrystEngComm* **2014**, *16*, 5989. (c) Xiong, W.-W.; Li, P.-Z.; Zhou, T.-H.; Tok, A. I. Y.; Xu, R.; Zhao, Y.; Zhang, Q. *Inorg. Chem.* **2013**, *52*, 4148.

(13) (a) Lin, H. Y.; Chin, C. Y.; Huang, H. L.; Huang, W. Y.; Sie, M. J.; Huang, L. H.; Lee, Y. H.; Lin, C. H.; Lii, K. H.; Bu, X.; Wang, S. L. *Science* **2013**, *339*, 811. (b) Kim, J. C.; Cho, K.; Ryoo, R. *Appl. Catal., A* **2014**, *470*, 420.

(14) Gao, J.; He, M.; Lee, Z. Y.; Cao, W.; Xiong, W. W.; Li, Y.; Ganguly, R.; Wu, T.; Zhang, Q. *Dalton Trans.* **2013**, *42*, 11367.

(15) (a) Martin, J. D.; Keary, C. L.; Thornton, T. A.; Novotnak, M. P.; Knutson, J. W.; Folmer, J. C. W. *Nat. Mater.* **2006**, *5*, 271. (b) Zhang, Q.; Chung, I.; Jang, J. I.; Ketterson, J. B.; Kanatzidis, M. G. *J. Am. Chem. Soc.* **2009**, *131*, 9896. (c) Biswas, K.; Zhang, Q.; Chung, I.; Song, J.-H.; Androulakis, J.; Freeman, A.; Kanatzidis, M. *J. Am. Chem. Soc.* **2010**, *132*, 14760. (d) Samarasekere, P.; Wang, X.; Jacobson, A. J.; Tapp, J.; Möller, A. *Inorg. Chem.* **2014**, *53* (1), 244.

(16) Bai, Y. L.; Tao, J.; Huang, R. B.; Zheng, L. S. *Angew. Chem., Int. Ed.* **2008**, *47*, 5344.

(17) (a) Zheng, S. T.; Wu, T.; Zuo, F.; Chou, C.; Feng, P.; Bu, X. *J. Am. Chem. Soc.* **2012**, *134*, 1934−7. (b) Gao, L.; Li, C. Y.; Yung, H.; Chan, K. Y. *Chem. Commun.* **2013**, *49*, 10629. (c) Srirambalaji, R.; Hong, S.; Natarajan, R.; Yoon, M.; Hota, R.; Kim, Y.; Ho, K. Y.; Kim, K. *Chem. Commun.* **2012**, *48*, 11650. (d) Ferey, G.; Mellot-Draznieks, C.; Serre, C.; Millange, F.; Dutour, J.; Surble, S.; Margiolaki, I. *Science* **2005**, *309*, 2040.

(18) (a) Dhakshinamoorthy, A.; Alvaro, M.; Garcia, H. *Catal. Sci. Technol.* **2011**, *1*, 856. (b) Cho, S. H.; Ma, B.; Nguyen, S. T.; Hupp, J. T.; Albrecht-Schmitt, T. E. *Chem. Commun.* **2006**, 2563. (c) Farha, O. K.; Shultz, A. M.; Sarjeant, A. A.; Nguyen, S. T.; Hupp, J. T. *J. Am. Chem. Soc.* **2011**, *133*, 5652. (d) Shultz, A. M.; Farha, O. K.; Hupp, J. T.; Nguyen, S. T. *Chem. Sci.* **2011**, *2*, 686. (e) Song, F. J.; Wang, C.; Falkowski, J. M.; Ma, L. Q.; Lin, W. B. *J. Am. Chem. Soc.* **2010**, *132*, 15390. (f) Zheng, M.; Liu, Y.; Wang, C.; Liu, S. B.; Lin, W. B. *Chem. Sci.* **2012**, *3*, 2623. (g) Tonigold, M.; Lu, Y.; Bredenkötter, B.; Rieger, B.; Bahnmüller, S.; Hitzbleck, J.; Langstein, G.; Volkmer, D. *Angew. Chem., Int. Ed.* **2009**, *48*, 7546. (h) Zhang, J.; Biradar, A. V.; Pramanik, S.; Emge, T. J.; Asefa, T.; Li, J. *Chem. Commun.* **2012**, *48*, 6541. (i) Berier, M. J.; Wharmby, W. K. M. T.; Kissner, R.; Kimmerle, B.; Wright, P. A.; Grunwaldt, J. D.; Baiker, A. *Chem.—Eur. J.* **2012**, *18*, 887.

(19) (a) Tang, Q.; Zhang, Q.; Wu, H.; Wang, Y. *J. Catal.* **2005**, *230*, 384. (b) Tang, Q.; Wang, Y.; Liang, J.; Wang, P.; Zhang, Q.; Wan, H. *Chem. Commun.* **2004**, 440.

(20) Remarks: Although the reaction conditions are different in detail such as the oxidant, reaction temperature, and time, comparison still shows the advantage of **NTU-Z30**. For example, for the catalyst $[Mn(\mu\text{-terph})(H_2O)_2]_n$, PW_x/MIL-101, and $[Co(Hoba)_2]$, the oxidants applied are hydroperoxide or *tert*-butyl hydroperoxide, which are not as green as molecular oxygen. Moreover, with similar molar ratios between cobalt and reactant and reaction conditions even with smaller flow rate of O_2 (30 mL min^{-1}) in our work, a higher TOF was obtained, indicating the superior catalytic activity of **NTU-Z30** as the heterogeneous catalyst.

(21) Monfared, H.; Mohajeri, A.; Morsali, A.; Janiak, C. *Monatsh. Chem. Verw. Teile Anderer Wiss. Chem. Mon.* **2009**, *140*, 1437.

(22) Chalati, T.; Horcajada, P.; Gref, R.; Couvreur, P.; Serre, C. *J. Mater. Chem.* **2011**, *21*, 2220.

(23) Jones, R. D.; Summerville, D. A.; Basolo, F. *Chem. Rev.* **1979**, *79*, 139.

(24) Meseguer, S.; Tena, M. A.; Gargori, C.; Badenes, J. A.; Llusar, M.; Monrós, G. *Ceram. Int.* **2007**, *33*, 843.